iJRASET
International Journal For Research in Applied Science and Engineering Technology

INTERNATIONAL JOURNAL FOR RESEARCH

IN APPLIED SCIENCE & ENGINEERING TECHNOLOGY

Volume: 12 **Issue:** VII **Month of publication:** July 2024

DOI: https://doi.org/10.22214/ijraset.2024.63524

www.ijraset.com

Call: 08813907089 | E-mail ID: ijraset@gmail.com

International Journal for Research in Applied Science & Engineering Technology (IJRASET)
ISSN: 2321-9653; IC Value: 45.98; SJ Impact Factor: 7.538
Volume 12 Issue VII July 2024- Available at www.ijraset.com

Deep Learning-Based Prediction of COVID-19 and Viral Pneumonia from Chest X-Ray Images

S. Peruvazhuthi[1], K. Praveen[2]
Department of Electronics and Communication Engineering, College of Engineering, Guindy, Anna University

Abstract: ***In recent times, the novel Coronavirus disease (COVID-19) has emerged as one of the most infectious diseases, causing significant public health crises across over 200 nations worldwide. Given the challenges associated with the time-consuming and error-prone nature of detecting COVID-19 through Reverse Transcription-Polymerase Chain Reaction (RT-PCR), there is a growing reliance on alternative methods, such as examining chest X-ray (CXR) images. Viral pneumonia symptoms include a persistent cough with mucus, fever, chills, shortness of breath, and chest pain, especially during deep breaths or coughing. These symptoms often overlap significantly with those of other respiratory infections, including COVID-19. Accurately predicting COVID-19 severity and distinguishing it from viral pneumonia is crucial for effective patient management. Deep learning models offer promise in automating this process. The chest X-ray (CXR) images undergo preprocessing through Contrast Limited Adaptive Histogram Equalization (CLAHE) to improve their quality. These enhanced images are fed into ResNet50 and EfficientNet-B0, both renowned deep learning models. Comparative evaluation demonstrates ResNet50 achieving an accuracy of 92.58%, whereas EfficientNet-B0 achieves a higher accuracy of 93.08%. This study underscores the efficacy of deep learning in COVID-19 prediction. The findings suggest EfficientNet-B0's potential for improved diagnostic accuracy. This methodology presents a promising approach for automated, accurate COVID-19 severity prediction and differentiation from viral pneumonia, aiding timely medical interventions.***

Keywords: ***Coronavirus disease, Reverse Transcription-Polymerase Chain Reaction, chest X-ray, Viral pneumonia, Deep learning models***

I. INTRODUCTION

The global impact of the COVID-19 pandemic began with a significant outbreak in December 2019 in Wuhan, China, caused by the zoonotic coronavirus SARS-CoV-2. It quickly spread worldwide, resulting in approximately 70 crore confirmed cases and a significant number of deaths from Jan 2020 to May 2024, according to Worldometer data. COVID-19 is a contagious respiratory illness that affects the respiratory system, with initial symptoms such as fever, cough, and difficulty breathing typically appearing between two to fourteen days after exposure. The severity of the illness varies depending on the individual's immune response and the intensity of the disease. The virus can spread from infected individuals both before symptoms appear and for 10 to 20 days afterward. Its ability to cross international borders has had a profound impact, affecting populations across the globe.

Viral pneumonia is an infection of the lungs caused by various viruses, such as influenza, Respiratory Syncytial Virus (RSV), adenovirus, and others. It is less likely to respond to antibiotics and often requires different treatment approaches. This type of pneumonia is more common during the fall and winter months and can affect individuals of all ages, though it is particularly dangerous for young children, the elderly, and people with weakened immune systems. Symptoms includes cough, often producing mucus, fever and chills, shortness of breath. The gold standard for diagnosing COVID-19 is the Reverse Transcription Polymerase Chain Reaction (RT-PCR) test, which detects the viral ribonucleic acid (RNA) of SARS-CoV-2. A positive PCR test confirms a COVID-19 diagnosis. For the COVID-19 cases, Chest X-rays show bilateral, peripheral ground-glass opacities or consolidation. The viral pneumonias might show different patterns, such as localized opacities or diffuse infiltrates. Deep learning (DL) is a subset of machine learning known for its effectiveness across various applications [1]. DL models, which consist of multilayered neural network architectures, excel at extracting intricate features from images and have proven invaluable in tasks such as biomedical disease detection [2]. For instance, they are adept at identifying conditions like diabetes and pneumonia from CT scans, significantly enhancing computer-aided diagnosis systems [3]. Convolutional neural networks (CNNs) are particularly favoured for their robust performance in detecting and classifying COVID-19, capable of handling complex datasets and classifying patients according to disease risk. Transfer learning has emerged as a potent technique in COVID-19 detection [4-6], leveraging pretrained neural networks like DenseNet201, MobileNetV2, ResNet18, ResNet50, ResNet101, VGG16, and VGG19 on extensive datasets of X-ray images [7].

These models excel in learning comprehensive features from diverse image datasets, enabling effective generalization even when COVID-19 data is limited. This approach addresses challenges related to data scarcity, facilitating quicker and more accurate diagnoses.

II. LITERATURE SURVEY

Panwar et al. [8] introduced a CNN-based method for detecting COVID-19 using binary classification of chest X-ray images (CXR), achieving an overall accuracy of approximately 88.10%. In contrast, Hemdan et al. [9] explored various deep learning algorithms for COVID-19 image classification, highlighting DenseNet's highest accuracy at 90%. Further investigations into deep learning models for COVID-19 detection [10] demonstrated varied performances among DenseNet121, VGG16, Xception, EfficientNet-B7, and NASNet, with EfficientNet-B7 leading with an accuracy of 92.48%. Another study [11] focused on early detection of COVID-19 using chest X-rays (CXR), employing VGG16 and ResNet50 for feature extraction. These models classified images into three groups—viral pneumonia, normal, and COVID-19—achieving average accuracies of 89.34% for VGG16 and 91.39% for ResNet50 in detecting COVID-19 cases from a dataset comprising 15,153 images.

In [12], researchers employed transfer learning with well-known architectures including CheX-Net, DenseNet, VGG19, MobileNet, InceptionV3, ResNet18, ResNet101, and SqueezeNet to classify chest X-ray (CXR) images into three categories: COVID-19, viral pneumonia, and normal. Their dataset consisted of 423 COVID-19 images, 1,485 viral pneumonia images, and 1,575 normal images, achieving an impressive accuracy of 91.94% in distinguishing between these classes.In [13], the authors conducted a comprehensive evaluation of classic and specialized models using a COVID-19 dataset. Classic models such as VGG19, ResNet50, MobileNetV2, InceptionV3, Xception, and DenseNet121 were compared alongside specialized models like DarkCOVIDNet and COVID-Net. Their findings highlighted ResNet50's superior performance, achieving notable accuracies of 93.20% in binary classification (COVID-19 and No COVID-19) and 86.13% in multi-class classification (COVID-19, No COVID-19, and Pneumonia) with a simple modification. These results underscore ResNet50's effectiveness in COVID-19 detection and differentiation from pneumonia, emphasizing its potential as a valuable tool in medical diagnostics.

In their study detailed in [13], researchers extensively evaluated both traditional and specialized models using a COVID-19 dataset. They compared classic models such as VGG19, ResNet50, MobileNetV2, InceptionV3, Xception, and DenseNet121 alongside specialized models like DarkCOVIDNet and COVID-Net. Their findings demonstrated that ResNet50 consistently outperformed other models, showing superior performance. With a simple adjustment, ResNet50 achieved impressive accuracies of 93.20% in binary classification (COVID-19 vs. No COVID-19) and 86.13% in multi-class classification (COVID-19, No COVID-19, and Pneumonia). These results underscore the effectiveness of ResNet50 in detecting COVID-19 and distinguishing it from pneumonia, highlighting its potential as a valuable tool in medical diagnostics. The studies cited illustrate the promising application of deep learning techniques, particularly transfer learning, in enhancing the detection of COVID-19 from chest X-ray images. These methods often involve refining pre-trained models to enhance detection accuracy. Overall, these findings emphasize the importance of leveraging advanced deep learning approaches to address crucial healthcare challenges, especially in the context of COVID-19 detection using medical imaging.

III. METHODOLOGY

Initially, the chest X-ray (CXR) images undergo preprocessing using Contrast Limited Adaptive Histogram Equalization (CLAHE), a technique employed to enhance image contrast and detail. Subsequently, the preprocessed images are resized to a standardized dimension and normalized, ensuring consistent pixel values across all images for optimal model performance.

The enhanced images are then subjected to feature extraction and classification using pre-trained architectures, including ResNet50 and EfficientNetB0. These architectures leverage their learned representations from extensive datasets to extract relevant features and classify the images into respective categories, such as COVID-19, pneumonia, and normal cases. Fig. 1 depicts the process of COVID-19 & pneumonia prediction.

A. Dataset

The COVID-19 Radiography Database [14,15], utilized as the main dataset, includes chest X-ray images from patients diagnosed with COVID-19, pneumonia, and those with normal lung conditions. Created in 2020 through a collaboration between Qatar University in Doha, Qatar, and the University of Dhaka in Bangladesh, alongside medical practitioners from Pakistan and Malaysia, the database was released gradually and comprises a total of 15,153 images. Within this dataset, there are 3,616 images depicting COVID-19 cases, 1,345 images showing viral pneumonia, and 10,192 images representing normal lung conditions.

Fig. 2 illustrates samples of (a) Normal, (b) COVID-19, and (c) Viral pneumonia images.

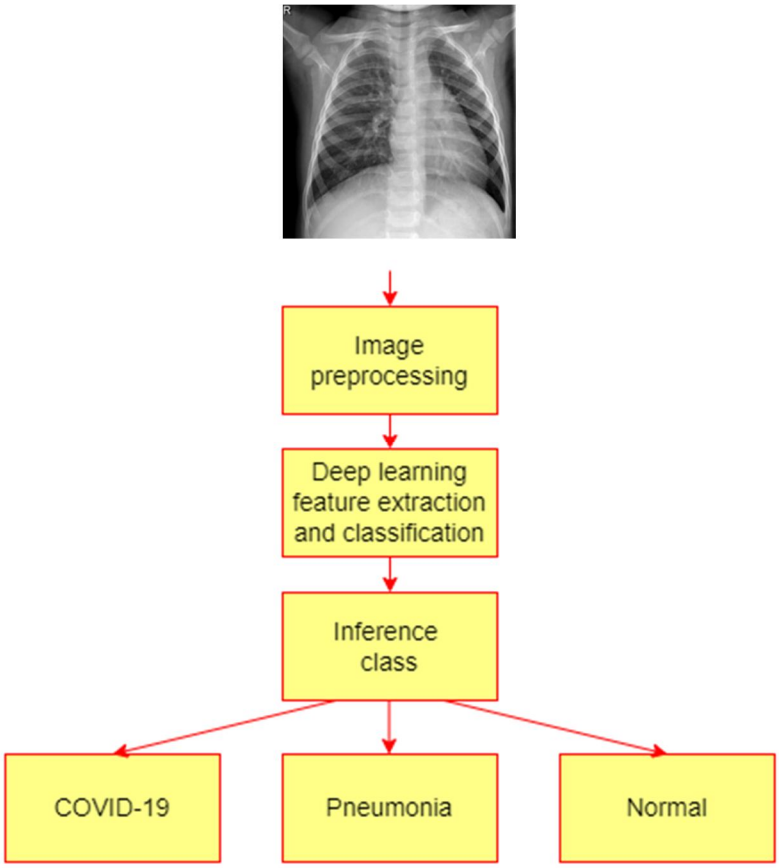

Fig. 1 Process of COVID-19 & pneumonia prediction.

B. Image Downsampling

Downsampling is a common technique used in machine learning and data analysis to mitigate class imbalance. It involves reducing the number of samples in the majority class to align with the number of samples in the minority class. This approach helps prevent bias in predictive modeling towards the majority class, thereby enhancing the accuracy of machine learning algorithms, particularly in tasks like classification where imbalanced datasets can lead to inaccurate predictions.

In the COVID-19 Radiography Database, down sampling was implemented to address an initial imbalance in the number of images across the three classes: COVID-19, viral pneumonia, and normal lung conditions. Initially, the dataset had varying numbers of images per class. By downsampling, the number of images for COVID-19 and normal lung conditions was decreased to match the number of images for viral pneumonia, which was set at 1,345 images. This adjustment ensured a more balanced representation of classes in the dataset, thereby improving the robustness and fairness of subsequent machine learning analyses and models trained on this data.

C. Image Preprocessing

Image preprocessing is crucial for improving the quality and usability of image data in deep learning algorithms. It involves applying specific techniques to raw image inputs to make them more appropriate for training deep neural networks. Three fundamental preprocessing techniques widely used in deep learning applications are CLAHE (Contrast Limited Adaptive Histogram Equalization), resizing, and normalization.

These methods prepare image data by improving contrast, standardizing dimensions, and scaling pixel values, respectively. By implementing these preprocessing steps, images are optimized for better performance and accuracy in tasks such as image classification and object detection.

(a) Normal

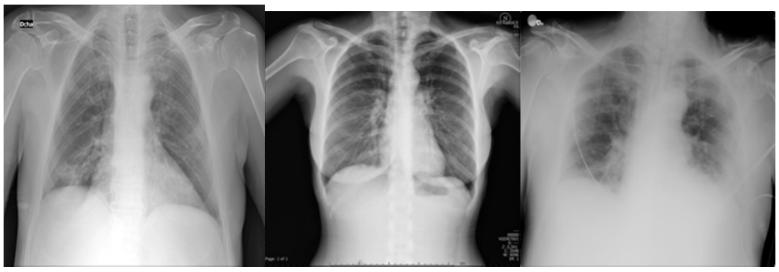

(b) COVID-19

(c) Viral pneumonia

Fig. 2 Images of (a) Normal (b) COVID-19 (c) Viral pneumonia

1) CLAHE (Contrast Limited Adaptive Histogram Equalization)

CLAHE (Contrast Limited Adaptive Histogram Equalization) is extensively used in image processing to enhance image quality by focusing on local contrast improvement. This method effectively enhances image clarity and detail sharpness while minimizing noise amplification.

The CLAHE algorithm comprises three main stages: tile generation, histogram equalization, and bilinear interpolation. Initially, the input image is divided into non-overlapping sections known as tiles. Subsequently, histogram equalization is applied to each tile using a specified clip limit.

Histogram equalization involves several steps including histogram computation, excess calculation, excess distribution, excess redistribution, and scaling and mapping using a cumulative distribution function (CDF). Fig. 3 represents the operation of CLAHE. Initially, the histogram of each tile in the input image is computed and divided into bins. Values exceeding a specified clip limit are redistributed across other bins. Subsequently, a Cumulative Distribution Function (CDF) is computed based on these histogram values.

The CDF values for each tile are then scaled and mapped to adjust the pixel values of the input image. The resulting tiles are combined using bilinear interpolation to generate an output image with improved contrast.

The extent of contrast enhancement in CLAHE is controlled by the clip limit, which determines how the histogram is clipped to mitigate noise and enhance contrast. A clip limit of 2.0 is often chosen to strike a balance between effective contrast enhancement and the risk of introducing artifacts.

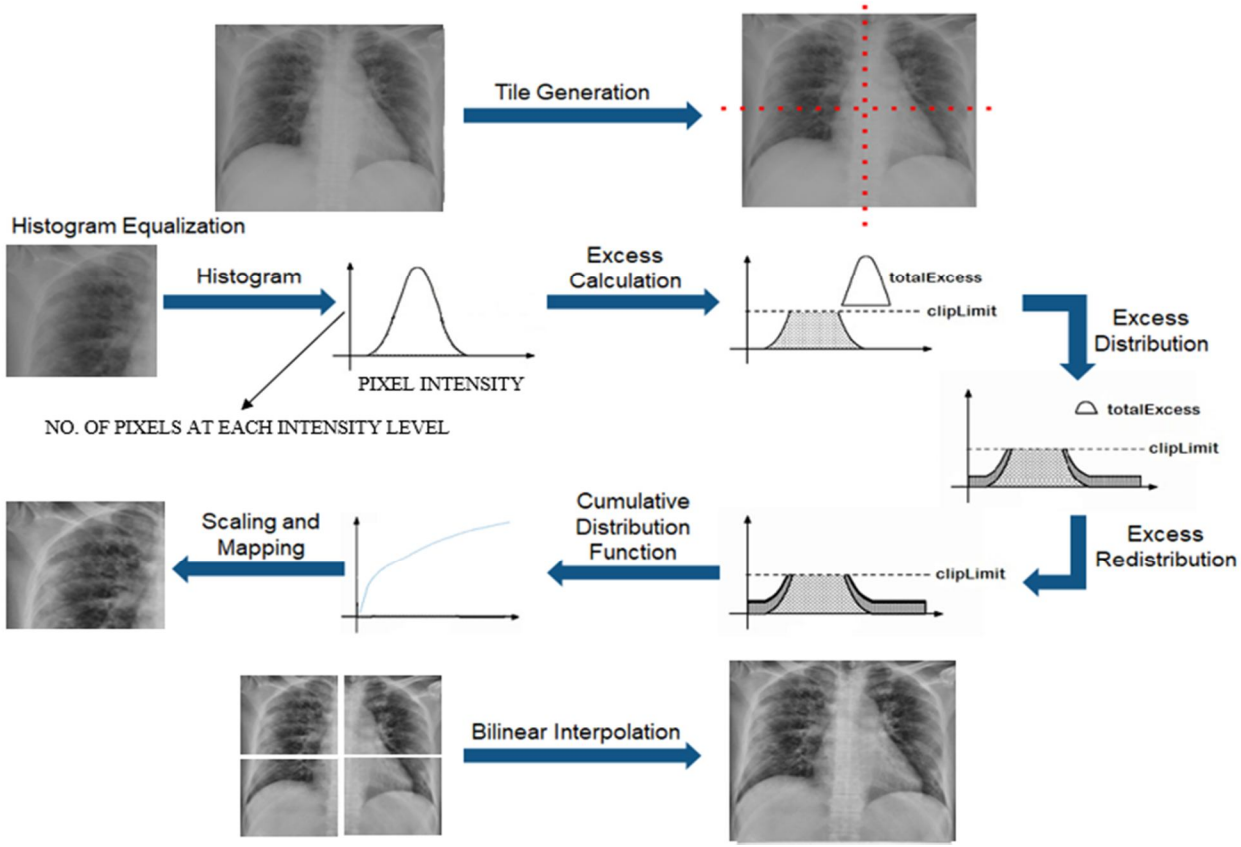

Fig. 3 CLAHE operation

Higher clip limits can lead to excessive enhancement and noise, while lower limits may result in insufficient contrast improvement. The selection of the clip limit is typically based on experimentation and the specific characteristics of the image dataset to achieve optimal enhancement while minimizing unwanted effects. Furthermore, a tile grid size of (8×8) is commonly used in CLAHE operations. This size is chosen for its ability to efficiently balance computational resources while effectively enhancing local contrast in images.

$$L^* = 116 \cdot f\left(\frac{Y}{Y_n}\right) - 16 \quad (1)$$

$$a^* = 500 \left[f\left(\frac{X}{X_n}\right) - f\left(\frac{Y}{Y_n}\right)\right] \quad (2)$$

$$b^* = 200 \left[f\left(\frac{Y}{Y_n}\right) - f\left(\frac{Z}{Z_n}\right)\right] \quad (3)$$

$$R' = \begin{cases} 12.92R & if\ R \le 0.0031308 \\ 1.055\ R^{1/2.4} - 0.055 & otherwise \end{cases} \quad (4)$$

$$G' = \begin{cases} 12.92G & if\ G \le 0.0031308 \\ 1.055\ G^{\frac{1}{2.4}} - 0.055 & otherwise \end{cases} \quad (5)$$

$$B' = \begin{cases} 12.92B & if\ B \le 0.0031308 \\ 1.055\ B^{1/2.4} - 0.055 & otherwise \end{cases} \quad (6)$$

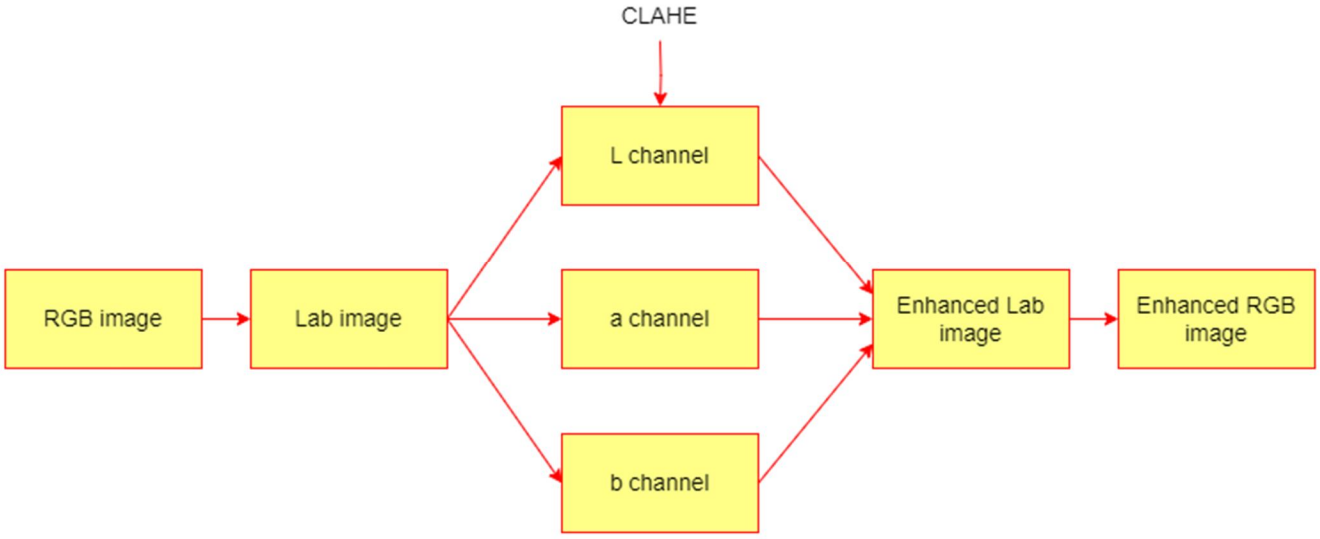

Fig. 4 Image enhancement process

The image enhancement process, as depicted in Fig. 4, involves transforming the RGB image into the Lab color space for more uniform color representation compared to RGB, which relies on Red, Green, and Blue intensities. In this process, the Lab transformation initially converts the RGB image. Subsequently, the Lightness (L) channel is isolated and subjected to CLAHE to enhance its contrast. After enhancing the L channel, it is reintegrated with the color components a (green to red) and b (blue to yellow) to reconstruct an improved Lab image. Finally, this enhanced Lab image is converted back to RGB for visualization purposes. Eq. (1-3) outline the method for converting from RGB to Lab color space, while Eq. (4-6) describe the reverse conversion process from Lab back to RGB. This approach ensures that the image undergoes effective contrast enhancement while preserving color fidelity and ensuring accurate representation during the transformation between color spaces.

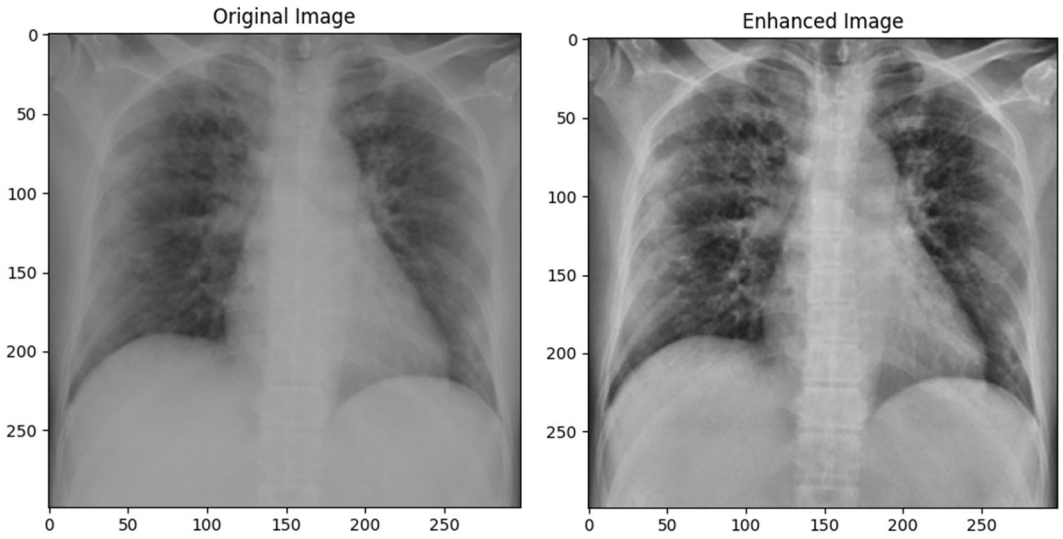

(a) (b)

Fig. 5 (a) Original image (b) Enhanced image

The original image and the image enhanced using CLAHE are presented in Fig. 5(a) and Fig. 5(b), respectively. These figures demonstrate the enhancement achieved based on CLAHE parameters.

2) Resizing

Resizing images after applying Contrast Limited Adaptive Histogram Equalization (CLAHE) is essential to ensure consistent dimensions, which is necessary for utilizing pretrained models effectively. CLAHE enhances contrast and image detail, but it may result in images of varying sizes. Resizing standardizes image dimensions to match model input requirements, often to a common size such as 224x224 pixels. It's important to maintain the aspect ratio during resizing to avoid distorting the image. While resizing is critical for improving computational efficiency during model inference, it can impact image resolution. Shrinking images to smaller dimensions may reduce detail, while enlarging them can lead to blurriness. Therefore, careful consideration of the resizing process is crucial to strike a balance between standardizing image inputs and preserving image quality.

3) Normalization

Normalization following resizing is a crucial preprocessing stage for preparing images for machine learning models. While resizing ensures consistent dimensions, normalization standardizes pixel values across images, which is essential for enhancing model stability and facilitating convergence during training. Post-resizing, normalization typically involves scaling pixel values to a standardized range, such as [0, 1]. This approach promotes model interpretability by ensuring uniform intensity ranges across all images.

D. RESNET50

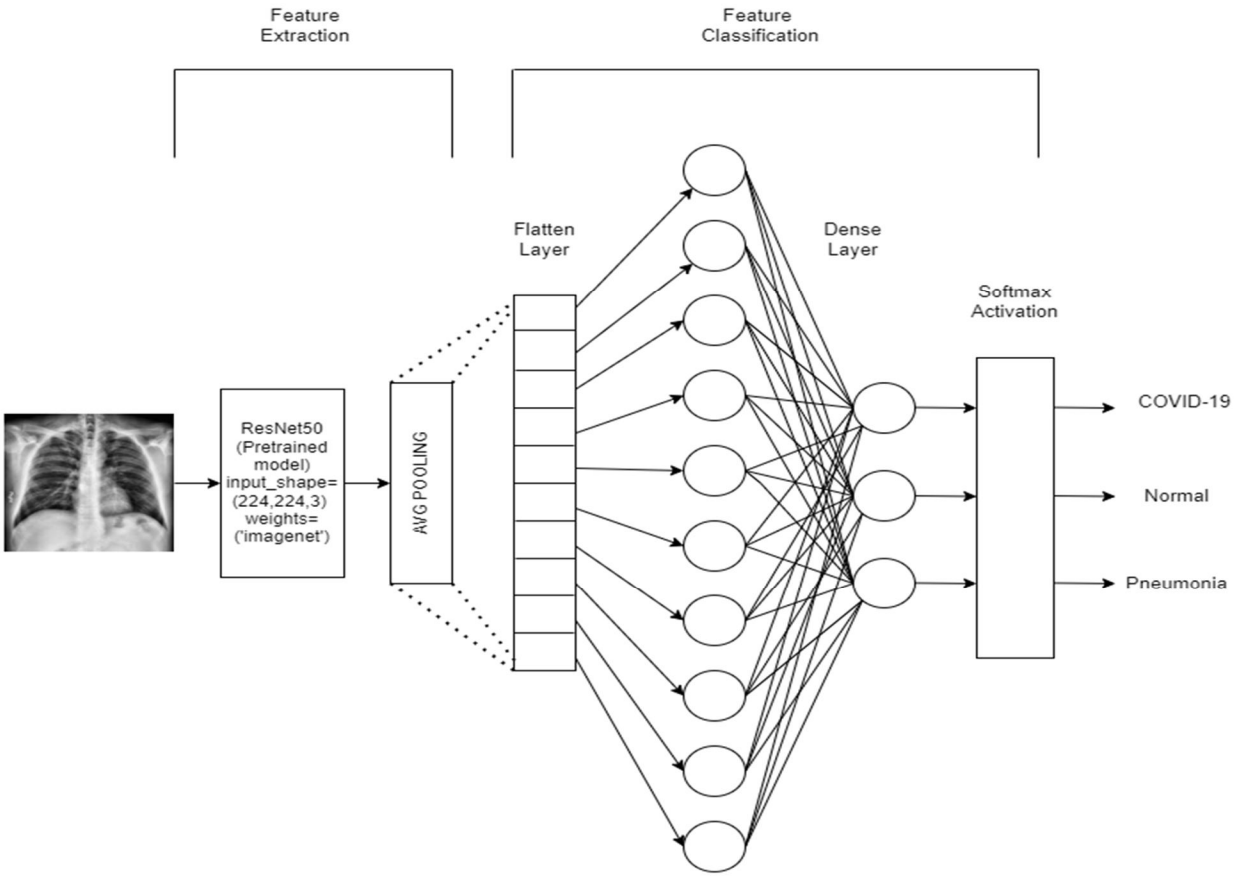

Fig. 6 Architecture of ResNet50

ResNet50, short for Residual Network with 50 layers, is a convolutional neural network architecture developed by Microsoft Research, has shown exceptional performance in various image classification tasks due to its depth and unique skip connection design. These skip connections, also known as residual connections, help mitigate the vanishing gradient problem by facilitating direct information flow between layers.

This architecture, detailed in Fig. 6, comprises convolutional and max pooling layers followed by fully connected layers for classification. Residual connections in ResNet50 enable the network to learn residual mappings, simplifying the optimization of very deep networks by allowing easier training compared to directly approximating the desired mapping. This design innovation contributes to smoother optimization and faster convergence during training. Softmax function for a vector of raw scores $\vec{z} = z_1, z_2, \ldots, z_k$ is given in the Eq. (7)

$$\sigma(\vec{z})_i = \frac{e^{z_i}}{\sum_{j=1}^{K} e^{z_j}} \quad (7)$$

E. Efficientnet-B0

EfficientNet-B0 is a convolutional neural network (CNN) architecture belonging to the EfficientNet family, renowned for its efficient utilization of computational resources alongside top-tier performance in image classification tasks. Serving as the foundational model in the EfficientNet series, EfficientNet-B0 is meticulously designed to strike a balance among model size, computational efficiency, and accuracy. It distinguishes itself through a novel scaling method that optimizes both depth and width of the network effectively. This scaling approach enables EfficientNet-B0 to achieve state-of-the-art accuracy using fewer parameters, thereby ensuring superior performance while conserving computational resources. These characteristics make EfficientNet-B0 particularly well-suited for applications where resource constraints are a consideration. Fig. 7 illustrates the architecture of EfficientNet-B0, while Eq. (8) defines the ReLU activation function used in the model.

$\text{ReLU}(x) = \max(0, x)$

x is the input to a neuron. (8)

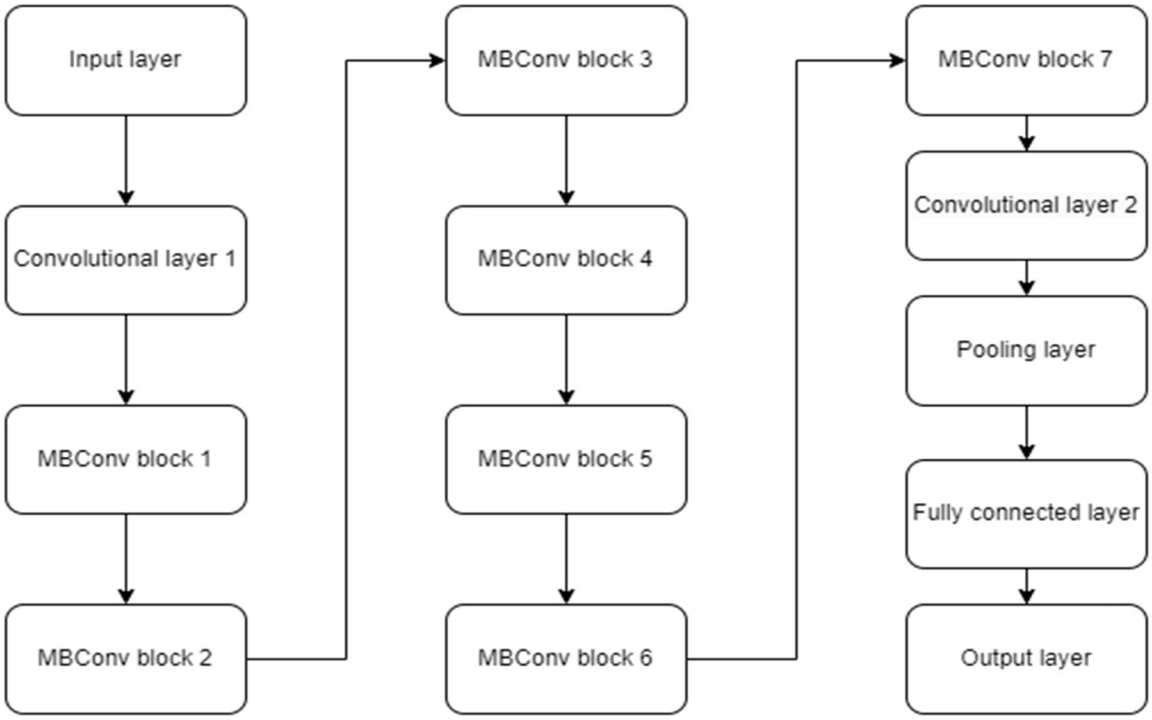

Fig. 7 Structure of EfficientNet-B0

IV. RESULTS AND DISCUSSION

For this work, a dataset comprising a total of 4035 images was utilized, with an 80:20 split for training and validation. This allocation resulted in 3228 images being designated for training the model, enabling the deep learning algorithm to learn from a diverse range of data. Additionally, 807 images were reserved for validation purposes, allowing for thorough evaluation of the model's performance and generalization capabilities on unseen data.

This distribution ensures both an adequate amount of data for training and a robust assessment of model performance during validation. The following performance metrics have been calculated for each model to evaluate their effectiveness.

1) Accuracy

It calculates the ratio of correctly predicted instances to the total number of instances in a dataset. Eq. (9) gives the accuracy score.

$$Accuracy = \frac{TP + TN}{TP + FP + TN + FN} \quad (9)$$

2) Precision

It measures the ability of the model to correctly detect true positives among all instances it predicted as positive. Eq. (10) gives the precision of the model.

$$Precision = \frac{TP}{TP + FP} \quad (10)$$

3) Recall

Recall also known as sensitivity or True Positive Rate (TPR) measures the ratio of actual positive classes that are correctly predicted. Recall of the model is described in Eq. (11).

$$Recall = \frac{TP}{TP + FN} \quad (11)$$

4) F1 score

It is expressed as the harmonic average of precision and recall of the model with a desirable value of 1 and an undesirable value of 0. Eq. (12) provides the F1 score of the model.

$$F1\ Score = 2 * \frac{Precision * Recall}{Precision + Recall} \quad (12)$$

The accuracy plot presented in the fig. 8 (a) and (b) shows the training progress and validation performance of both the ResNet50 and EfficientNet-B0 models across ten epochs. It provides a clear visualization of how effectively each model classifies COVID-19, pneumonia, and normal cases based on medical images. For ResNet50, the plot shows a steady increase in both training and validation accuracies, with occasional fluctuations indicating potential instability or overfitting. The model achieves its highest validation accuracy of 92.58%, demonstrating strong capability in distinguishing between different medical conditions. Similarly, the accuracy plot for EfficientNet-B0 depicts consistent improvements in training and validation accuracies over the epochs. The plot shows a notable achievement of 93.08% validation accuracy by the tenth epoch.

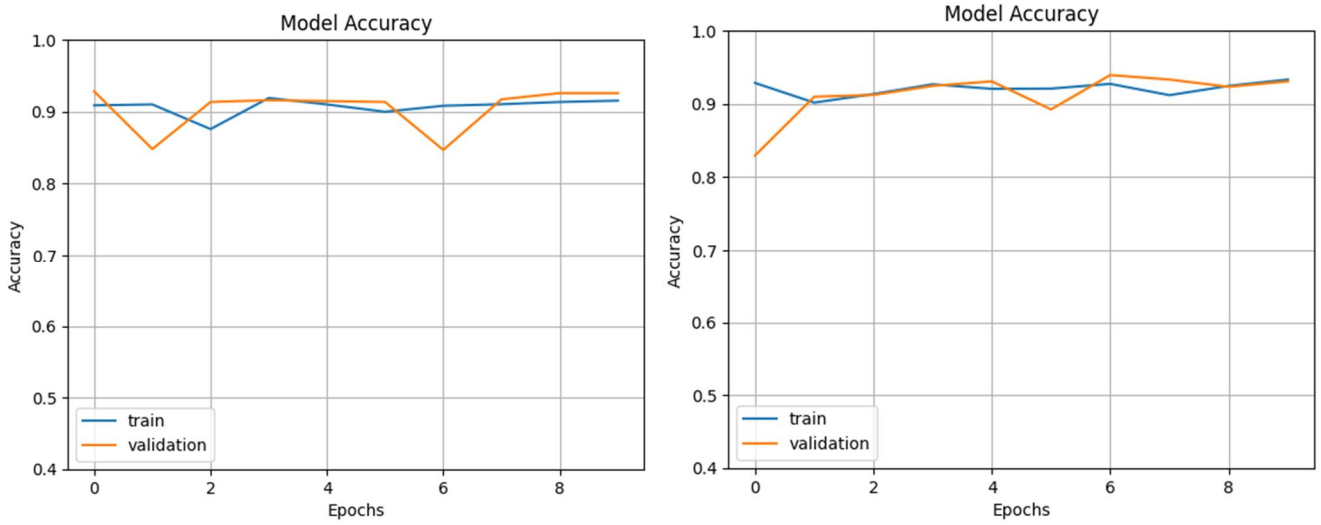

(a) (b)

Fig. 8 Accuracy plot of (a) Resnet50 and (b) Efficientnet-B0

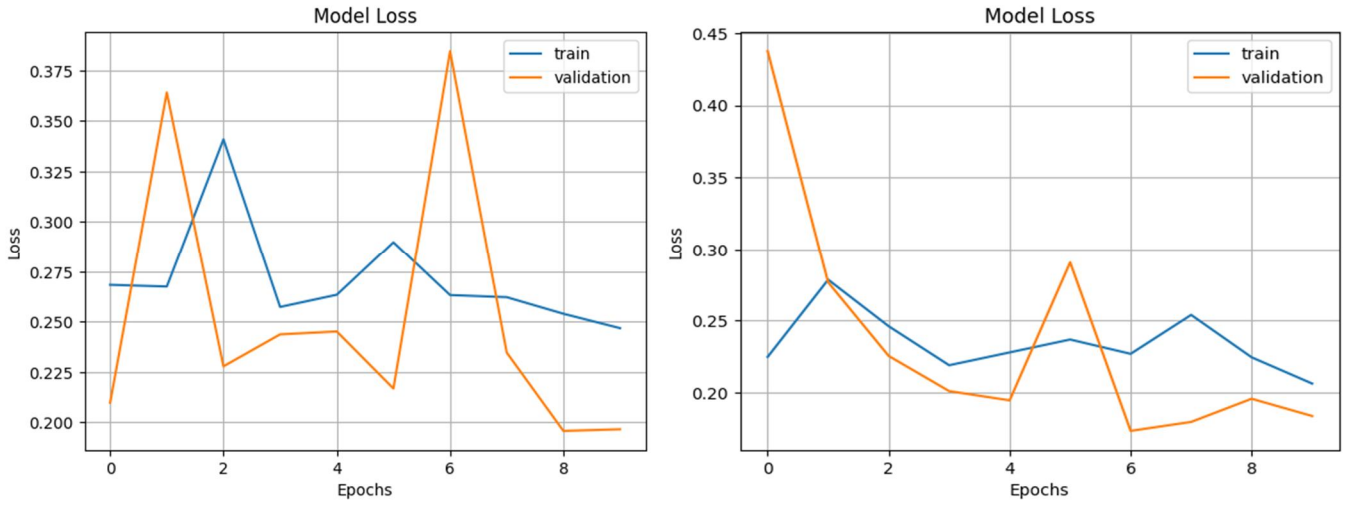

(a) (b)

Fig. 9 Loss plot of (a) Resnet50 and (b) Efficientnet-B0

The loss plot in the Fig. 9 (a) and (b) provides a visual representation of how the ResNet50 and EfficientNet-B0 models progress in minimizing prediction errors across ten training epochs. It serves as a critical metric for assessing the models' performance in relation to their ability to reduce discrepancies between predicted and actual labels. For ResNet50, the loss plot shows a consistent decrease in both training and validation losses over the epochs. This trend indicates that the model effectively learns and improves its accuracy in classifying COVID-19, pneumonia, and normal cases. Occasional fluctuations in the loss values may occur, but the overall trajectory demonstrates the model's capability to minimize prediction errors and enhance its classification accuracy. Similarly, the loss plot for EfficientNet-B0 illustrates a gradual decline in both training and validation losses throughout the training process. This pattern reflects the model's continuous improvement in minimizing errors and optimizing its classification performance across medical image datasets.

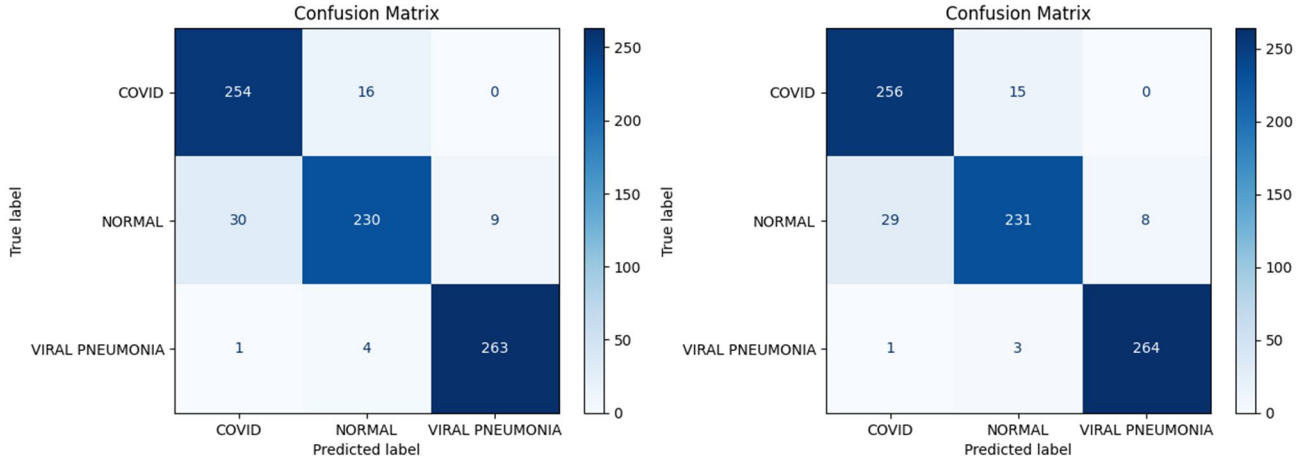

(a) (b)

Fig. 10 Confusion matrix of (a) Resnet50 and (b) Efficientnet-B0

The confusion matrix is a valuable tool for evaluating the performance of a classification model, particularly in multiclass scenarios where there are more than two possible outcomes. Each row of the matrix represents the actual classes, while each column represents the predicted classes. The purpose of the confusion matrix is to provide insights into the model's ability to correctly classify instances across all classes and to identify any patterns of misclassification. The confusion matrices presented in Figures 10 (a) and 10 (b) depict the performance evaluation of a classification model across three classes: class 1 (e.g., COVID-19), class 2 (e.g., normal), and class 3 (e.g., pneumonia).

In both matrices, each row and column correspond to specific class labels, where diagonal elements indicate correct classifications and off-diagonal elements represent misclassifications. In Figure 10 (a), the model shows strong performance with 254 instances of class 1 correctly classified, 230 instances of class 2 correctly classified, and 263 instances of class 3 correctly classified. However, there are instances of misclassification, such as 16 instances of class 1 misclassified as class 2 and 30 instances of class 2 misclassified as class 1. Similarly, in Figure 10 (b), the model correctly classifies 256 instances of class 1, 231 instances of class 2, and 264 instances of class 3, with 15 instances of class 1 misclassified as class 2 and 29 instances of class 2 misclassified as class 1. These matrices provide a detailed assessment of the model's strengths in correctly classifying certain classes and areas where improvements are needed to reduce misclassifications.

The performance comparison between the ResNet50 and EfficientNet-B0 models reveals differences in their classification capabilities. The ResNet50 model achieved accuracy, precision, recall, and F1 scores of approximately 0.925, 0.926, 0.926, and 0.925, respectively. In contrast, the EfficientNet-B0 model demonstrated slightly superior performance, with accuracy, precision, recall, and F1 scores of 0.930, 0.9307, 0.9305, and 0.9297, respectively. This suggests that EfficientNet-B0 might be more adept at capturing and generalizing features from the data, leading to more accurate predictions.

V. CONCLUSION

This work aimed to enhance medical image quality using Contrast Limited Histogram Equalization (CLAHE) and then applied two prominent deep learning architectures, ResNet50 and EfficientNet-B0, for predicting COVID-19 and pneumonia. Experimental results showed ResNet50 achieving an accuracy of 92.58%, while EfficientNet-B0 surpassed it with 93.08%. These findings underscore the capability of deep learning models in accurately categorizing COVID-19 cases from medical images. However, the performance of these models can be influenced by factors like dataset size, image quality, and variations in disease presentation. Future research could explore new image enhancement techniques or incorporate additional preprocessing steps to further enhance model performance.

REFERENCES

[1] M.A. Talukder, M.M. Islam, M.A. Uddin, A. Akhter, M.A.J. Pramanik, S. Aryal, M.A.A. Almoyad, K.F. Hasan, and M.A. Moni, "An efficient deep learning model to categorize brain tumor using reconstruction and fine-tuning," Expert Syst. Appl., vol. 120534, 2023.
[2] M.A. Talukder, M.M. Islam, M.A. Uddin, A. Akhter, K.F. Hasan, and M.A. Moni, "Machine learning-based lung and colon cancer detection using deep feature extraction and ensemble learning," Expert Syst. Appl., vol. 205, pp. 117695, 2022.
[3] M. Zysman, J. Asselineau, O. Saut, E. Frison, M. Oranger, A. Maurac, J. Charriot, R. Achkir, S. Regueme, E. Klein, et al., "Development and external validation of a prediction model for the transition from mild to moderate or severe form of COVID-19," Eur. Radiol., pp. 1-13, 2023.
[4] N.D. Kathamuthu, S. Subramaniam, Q.H. Le, S. Muthusamy, H. Panchal, S.C.M. Sundararajan, A.J. Alrubaie, M.M.A. Zahra, "A deep transfer learning-based convolution neural network model for COVID-19 detection using computed tomography scan images for medical applications," Adv. Eng. Softw., vol. 175, pp. 103317, 2023.
[5] S. Agrawal, V. Honnakasturi, M. Nara, N. Patil, "Utilizing deep learning models and transfer learning for COVID-19 detection from X-Ray images," SN Comput. Sci., vol. 4, no. 4, pp. 326, 2023.
[6] M.M. Rana, M.M. Islam, M.A. Talukder, M.A. Uddin, S. Aryal, N. Alotaibi, S.A. Alyami, K.F. Hasan, and M.A. Moni, "A robust and clinically applicable deep learning model for early detection of Alzheimer's," IET Image Process., pp. 1–17, 2023.
[7] A. Subasi, T. Keles, F. Ozyurt, S. Dogan, T. Tuncer, "Feature extraction and fusion using deep convolutional neural networks for COVID-19 detection using CT and X-ray images," World J. Adv. Res. Rev., vol. 19, no. 1, pp. 914–933, 2023.
[8] H. Panwar, P. Gupta, M.K. Siddiqui, R. Morales-Menendez, V. Singh, "Application of deep learning for fast detection of COVID-19 in X-Rays using ncovnet," Chaos Solitons Fractals, vol. 138, pp. 109944, 2020.
[9] E.E.-D. Hemdan, M.A. Shouman, M.E. Karar, "Covidx-net: A framework of deep learning classifiers to diagnose COVID-19 in X-ray images," 2020, arXiv preprint arXiv:2003.11055.
[10] B. Nigam, A. Nigam, R. Jain, S. Dodia, N. Arora, B. Annappa, "COVID-19: Automatic detection from X-ray images by utilizing deep learning methods," Expert Syst. Appl., vol. 176, pp. 114883, 2021.
[11] N. S. Kavya, T. Shilpa, N. Veeranjaneyulu, and D. D. Priya, "Detecting Covid19 and pneumonia from chest X-ray images using deep convolutional neural networks," Materials Today: Proceedings, vol. 64, pt. 1, pp. 737-743, 2022. doi: 10.1016/j.matpr.2022.05.199.
[12] Q. Li, X. Guan, P. Wu, et al., "Early transmission dynamics in Wuhan, China, of novel coronavirus-infected pneumonia," N. Engl. J. Med., vol. 382, no. 13, pp. 1199–1207, 2020.
[13] S. Agrawal, V. Honnakasturi, M. Nara, N. Patil, "Utilizing deep learning models and transfer learning for COVID-19 detection from X-ray images," SN Comput. Sci., vol. 4, no. 4, pp. 326, 2023.
[14] M. E. H. Chowdhury, T. Rahman, A. Khandakar, R. Mazhar, M. A. Kadir, Z. B. Mahbub, K. R. Islam, M. S. Khan, A. Iqbal, N. Al-Emadi, M. B. I. Reaz, and M. T. Islam, "Can AI help in screening Viral and COVID-19 pneumonia?" IEEE Access, vol. 8, pp. 132665-132676, 2020.
[15] T. Rahman, A. Khandakar, Y. Qiblawey, A. Tahir, S. Kiranyaz, S. B. A. Kashem, M. T. Islam, S. A. Maadeed, S. M. Zughaier, M. S. Khan, and M. E. Chowdhury, "Exploring the Effect of Image Enhancement Techniques on COVID-19 Detection using Chest X-ray Images," 2020.

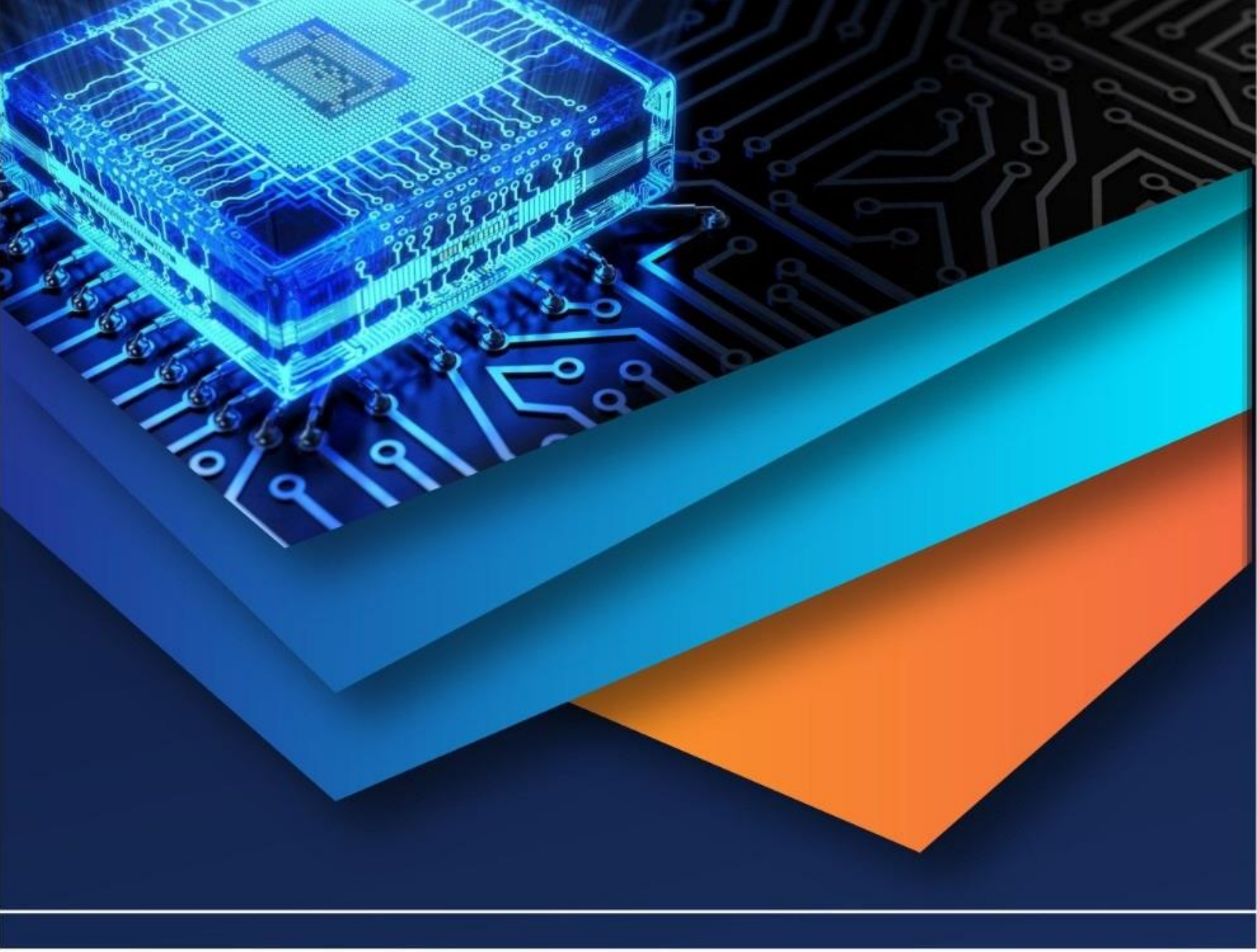

10.22214/IJRASET

45.98

IMPACT FACTOR: 7.129

IMPACT FACTOR: 7.429

INTERNATIONAL JOURNAL FOR RESEARCH

IN APPLIED SCIENCE & ENGINEERING TECHNOLOGY